

Determination of the ionization and dissociation energies of the deuterium molecule (D_2)

Jinjun Liu,¹ Daniel Sprecher,¹ Christian Jungen,² Wim Ubachs,³ and Frédéric Merkt^{1,a)}

¹Laboratorium für Physikalische Chemie, ETH-Zürich, 8093 Zürich, Switzerland

²Laboratoire Aimé Cotton, CNRS II, Bâtiment 505, Campus d'Orsay, 91405 Orsay Cedex, France

³Department of Physics and Astronomy, Laser Centre, Vrije Universiteit, De Boelelaan 1081, 1081 HV Amsterdam, The Netherlands

(Received 18 December 2009; accepted 9 March 2010; published online 15 April 2010)

The transition wave numbers from selected rovibrational levels of the $EF\ ^1\Sigma_g^+(v=0)$ state to selected np Rydberg states of ortho- and para- D_2 located below the adiabatic ionization threshold have been measured at a precision better than 10^{-3} cm^{-1} . Adding these wave numbers to the previously determined transition wave numbers from the $X\ ^1\Sigma_g^+(v=0, N=0, 1)$ states to the $EF\ ^1\Sigma_g^+(v=0, N=0, 1)$ states of D_2 and to the binding energies of the Rydberg states calculated by multichannel quantum defect theory, the ionization energies of ortho- and para- D_2 are determined to be $124\,745.394\,07(58)\text{ cm}^{-1}$ and $124\,715.003\,77(75)\text{ cm}^{-1}$, respectively. After re-evaluation of the dissociation energy of D_2^+ and using the known ionization energy of D , the dissociation energy of D_2 is determined to be $36\,748.362\,86(68)\text{ cm}^{-1}$. This result is more precise than previous experimental results by more than one order of magnitude and is in excellent agreement with the most recent theoretical value $36\,748.3633(9)\text{ cm}^{-1}$ [K. Piszczatowski, G. Łach, M. Przybytek *et al.*, *J. Chem. Theory Comput.* **5**, 3039 (2009)]. The ortho-para separation of D_2 , i.e., the energy difference between the $N=0$ and $N=1$ rotational levels of the $X\ ^1\Sigma_g^+(v=0)$ ground state, has been determined to be $59.781\,30(95)\text{ cm}^{-1}$. © 2010 American Institute of Physics. [doi:10.1063/1.3374426]

I. INTRODUCTION

The ionization and dissociation energies of the hydrogen molecule (H_2) and its isotopomers (D_2 and HD) are benchmark quantities in molecular quantum mechanics.^{1,2} Recently, we measured the transition wave number from the EF state of ortho- H_2 to a selected Rydberg state below the ground state of ortho- H_2^+ with a precision of $0.000\,29\text{ cm}^{-1}$.³ Combining this measurement with previous experimental and theoretical results for other energy intervals, the ionization and dissociation energies of the hydrogen molecule have been determined to be $124\,417.491\,13(37)$ and $36\,118.069\,62(37)\text{ cm}^{-1}$, respectively. Most recently, Piszczatowski *et al.*² made a new theoretical calculation of the dissociation energy of H_2 and D_2 by including nonadiabatic, relativistic, and quantum electrodynamics (QED) corrections. The relativistic and QED corrections were obtained at the adiabatic level of theory by including all contributions of the order α^2 and α^3 as well as the major (one-loop) α^4 term, where α is the fine-structure constant. The theoretical value they obtained for the dissociation energy of H_2 , $36\,118.0695(10)\text{ cm}^{-1}$, is in excellent agreement with our value. For the D_2 molecule, however, Piszczatowski *et al.* pointed out a small discrepancy (at the level of two standard deviations of the experimental value) between their theoretical value [$36\,748.3633(9)\text{ cm}^{-1}$] and the most recent experimental result [$36\,748.343(10)\text{ cm}^{-1}$, Ref. 4]. A new experimental determination of the dissociation energy of D_2 with a similar precision to that reached for H_2 would there-

fore be desirable to resolve this discrepancy and would provide another quantity with which future theoretical calculations can be compared.

We report here on a new determination of the ionization energies of both ortho- and para- D_2 [$E_i(\text{ortho-}D_2) \equiv E_i(D_2)$ and $E_i(\text{para-}D_2)$] from which we derive a new experimental value of the dissociation energy of D_2 . The ionization energies are obtained in each case as a sum of three energy intervals (see Fig. 1). In the case of ortho- D_2 , the first energy interval is between the $X\ ^1\Sigma_g^+(v=0, N=0)$ and the $EF\ ^1\Sigma_g^+(v=0, N=0)$ levels, the transition wave number of which was measured with high precision previously [$99\,461.449\,08(11)\text{ cm}^{-1}$, Ref. 5], the second between the $EF\ ^1\Sigma_g^+(v=0, N=0)$ and the $29p2_1(0)$ Rydberg state belonging to a series converging on the $X^+ \ ^2\Sigma_g^+(v^+=0, N^+=2)$ level of ortho- D_2^+ , and the third between the $29p2_1(0)$ Rydberg state and the $X^+ \ ^2\Sigma_g^+(v^+=0, N^+=0)$ ionic level. In the case of para- D_2 , the first energy interval is between the $X\ ^1\Sigma_g^+(v=0, N=1)$ and the $EF\ ^1\Sigma_g^+(v=0, N=1)$ levels [$99\,433.716\,38(11)\text{ cm}^{-1}$, Ref. 5], the second between the $EF\ ^1\Sigma_g^+(v=0, N=1)$ and the $52p1_2(0)$ Rydberg state belonging to a series converging on the $X^+ \ ^2\Sigma_g^+(v^+=0, N^+=1)$ level of para- D_2^+ , and the third the binding energy of the $52p1_2(0)$ Rydberg state. The transition wave numbers between the selected rovibrational levels of the EF state and the Rydberg states were measured using a $(2+1')$ resonant three-photon excitation sequence followed by delayed pulsed-field ionization (PFI) of the Rydberg states as in our study of H_2 .³ The binding energies of the Rydberg states were calculated by multichannel quantum defect theory (MQDT). The accuracy

^{a)}Electronic mail: feme@xuv.phys.chem.ethz.ch.

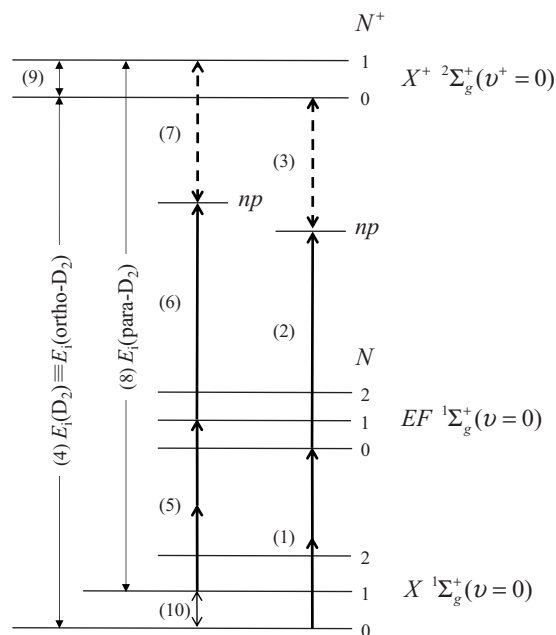


FIG. 1. Schematic energy level diagram of D_2 illustrating the procedure used to determine the ionization energies and the ortho-para separation. The energy intervals are not to scale. The bold arrows show the multiphoton excitation scheme used in the present experiment. The dashed arrows show the binding energies of the Rydberg states. The numerical values of the energy intervals (1)–(10) are given in Table III. The hyperfine structures of the different levels have not been drawn for clarity (see text for details).

of the MQDT calculations for D_2 has been verified independently in a comparison with a high-resolution measurement of the nf Rydberg spectra of D_2 by millimeter-wave spectroscopy⁶ and also with high-resolution laser spectra of the np Rydberg states (see below).

The dissociation energy of D_2 [$D_0(D_2)$] can be derived using the relation (see Fig. 5 of Ref. 3)

$$D_0(D_2) = E_i(D_2) + D_0(D_2^+) - E_i(D), \quad (1)$$

from the dissociation energy of the molecular cation [$D_0(D_2^+)$], which was re-evaluated using available literature data (see Appendix B), and the ionization energy of the atom [$E_i(D)$], which is known very accurately.⁷

In addition, the ortho-para separation of the neutral molecule ΔE_{1-0} , defined as the energy level separation between the $N=0$ and $N=1$ rotational energy levels of the $X^+ 1\Sigma_g^+(v=0)$ state of D_2 , can be derived using the relation (see Fig. 1):

$$\Delta E_{1-0} = E_i(\text{ortho-}D_2) + \Delta E_{1-0}^+ - E_i(\text{para-}D_2), \quad (2)$$

where ΔE_{1-0}^+ is the ortho-para separation of the cation, which is known very accurately from calculations.⁸

II. EXPERIMENT

The experimental setup is the same as used in our previous study of H_2 .³ In brief, the third harmonic of a commercial dye laser ($\lambda \sim 201$ nm, bandwidth ~ 0.04 cm^{-1}) was used to excite the $EF^+ 1\Sigma_g^+(v=0, N=0, 1) \leftarrow X^+ 1\Sigma_g^+(v=0, N=0, 1)$ two-photon transitions. The second harmonic of the near-infrared (NIR) output of a pulsed titanium-doped sapphire (Ti:Sa) amplifier ($\lambda \sim 396$ nm,

bandwidth ~ 20 MHz),^{9,10} seeded by a Ti:Sa cw ring laser, was then used to access np Rydberg states belonging to series converging on the lowest two rotational levels ($N^+=0$ or 1) of the $X^+ 2\Sigma_g^+(v^+=0)$ state of D_2^+ from the selected $EF^+ 1\Sigma_g^+(v=0, N=0$ or 1) levels. The 396 nm laser beam was split into two components and introduced into the interaction region in a counterpropagating configuration, both components overlapping spatially with the 201 nm beam. The difference between the transition wave numbers measured using each of these two components represents twice the Doppler shift resulting from a possible nonorthogonality between the molecular beam and the 396 nm laser beams and can be eliminated by taking the average value of the two measurements. The transitions were detected by ionizing the Rydberg states created by the two-step process using a pulsed electric field applied with a time delay with respect to the laser pulses. The generated cations were extracted by the same field and accelerated toward a micro-channel plate detector. Spectra were obtained by monitoring the D_2^+ ion signal as a function of the wave number of the second laser.

The absolute and relative calibration of the Ti:Sa-cw-ring-laser frequency was carried out by recording, simultaneously with the PFI spectra, the Doppler-free saturation absorption spectrum of I_2 ^{3,5,11} and the transmission signal through a high-finesse Fabry–Pérot etalon locked to a polarization-stabilized He–Ne laser.¹² The frequency shift arising in the multipass amplification in the Ti:Sa crystals (<10 MHz) was determined by monitoring the interference between the pulse-amplified laser beam with the cw NIR output of the ring laser¹³ and taking the Fourier transform of the beat-note signal recorded when the 396 nm laser was on resonance with the EF to Rydberg transitions.

III. RESULTS

A. Survey spectra of Rydberg states and MQDT calculations

In our previous work on H_2 , the binding energy of the selected $54p1_1(0)$ Rydberg state of ortho- H_2 was taken from the result of a millimeter-wave spectroscopic experiment analyzed by MQDT at submegahertz accuracy.¹⁴ In a similar millimeter-wave experiment carried out on para- D_2 ,⁶ transitions from $n=51d-53d$ to $n=54f-57f$ Rydberg states belonging to series converging on the ground state of para- D_2^+ could also be measured and extrapolated to their series limits using the same MQDT parameters as used for ortho- H_2 at the same accuracy. These results confirmed the expectation that isotopic substitution does not affect the eigenquantum defects and demonstrated the ability of MQDT to predict the binding energy of Rydberg states with submegahertz accuracy.

No millimeter-wave transitions to the np states accessed in the present experiment were observed for para- D_2 . The binding energies of these np states were therefore calculated by MQDT in the present work, as listed in the second column of Table I. These values correspond to energy level separations between the centers of gravity of the hyperfine structures of both the Rydberg states and the $N^+=0$ ($N^+=1$)

TABLE I. Binding energies of the Rydberg states of ortho- D₂ (para-D₂) calculated by MQDT, their experimental wave numbers relative to the 29p2₁ (52p1₂) states determined from the survey spectra, and the binding energies of the 29p2₁ (52p1₂) states calculated as sums of these two quantities (in cm⁻¹).

Rydberg state $n\ell N_N^+$	MQDT binding energy	Experimental wave number relative to 29p2 ₁	Experimental binding energy of 29p2 ₁ ^a
ortho-D ₂			
50p0 ₁	44.193 51	-0.961 90(80)	43.231 61
29p2 ₁ ^b	43.232 89	0	43.232 89
51p0 ₁	42.014 44	1.217 20(80)	43.231 64
52p0 ₁	40.517 04	2.715 88(80)	43.232 92
53p0 ₁	39.051 17	4.181 28(80)	43.232 45
54p0 ₁	37.661 24	5.571 52(80)	43.232 76
55p0 ₁	36.370 53	6.862 34(80)	43.232 87
Standard deviation			0.000 58
Rydberg state $n\ell N_N^+$	MQDT binding energy	Experimental wave number relative to 52p1 ₂	Experimental binding energy of 52p1 ₂ ^a
para-D ₂			
24p3 ₂ ^b	45.104 08	-4.550 18(80)	40.553 90
50p1 ₂	43.666 74	-3.114 74(80)	40.552 00
51p1 ₂	42.096 42	-1.543 32(80)	40.553 10
52p1 ₂	40.552 23	0	40.552 23
53p1 ₂	39.073 74	1.478 74(80)	40.552 48
54p1 ₂	37.669 40	2.884 40(80)	40.553 80
55p1 ₂	36.339 05	4.213 60(80)	40.552 65
56p1 ₂	35.081 98	5.471 70(80)	40.553 68
57p1 ₂	33.898 69	6.655 06(80)	40.553 75
Standard deviation			0.000 74

^aCalculated by adding up the MQDT binding energy of each Rydberg state and its relative position (in cm⁻¹) with respect to the 29p2₁ (52p1₂) state of ortho-D₂ (para- D₂) determined in the survey spectra.

^bState with the largest contribution from the 29p2₁ (24p3₂) zero-order state. Because of the strong interaction between the $np0_1$ and $np2_1$ ($np1_2$ and $np3_2$) channels of ortho-D₂ (para-D₂), all Rydberg states are mixed.

level of ortho-D₂⁺ (para-D₂⁺). The hyperfine structure of the Rydberg states of para-D₂ was determined by MQDT in a full calculation of the type described in Refs. 6 and 14 and the hyperfine structure of para-D₂⁺ was taken from Ref. 6. The binding energies were found to be identical to within 1 MHz with the binding energies determined in MQDT calculations neglecting nuclear spins. For ortho-D₂ Rydberg states and ortho-D₂⁺, for which the hyperfine structure is not known, we have therefore determined the binding energy in MQDT calculations neglecting nuclear spins. These are also expected to be accurate within 1 MHz. One should note here that the hyperfine splittings of the np ($S=0$) states at $n < 60$ is extremely small (typically less than 5 MHz) because the exchange interaction is much larger than the hyperfine interaction.¹⁴ In the present calculation, the MQDT parameters are the same as those determined for H₂ in Ref. 14 and ionization channels associated with vibrational levels of the cation with $v^+ \leq 9$ were included. The energies of the ionic levels were taken from Ref. 8. The p Rydberg states are labeled $n\ell N_N^+(S)$ with all quantum numbers having their usual meanings (see Ref. 14 for details). A strong interaction between the $N^+=0$ and $N^+=2$ channels of ortho-D₂ and between the $N^+=1$ and $N^+=3$ channels of para-D₂ leads to the observation, for instance, of the 29p2₁ level in spectra of the $np0_1$ levels. This interaction is perfectly described by the MQDT calculations.

Although it has been proven that the same MQDT parameters can be used to describe the nf levels of both ortho-H₂ and para-D₂ with submegahertz accuracy,⁶ we decided to independently verify the accuracy of the calculations of np states of both ortho- and para-D₂. For this reason, we recorded the survey spectra of the np Rydberg series of ortho- and para-D₂ in the region close to the nd and nf states that were accessed in the previous millimeter-wave experiments.⁶ The spectra of ortho- and para-D₂ are displayed in Figs. 2(a) and 2(b), respectively, and consist each of one series of strong transitions from the $EF\ ^1\Sigma_g^+(v=0, N=0$ and 1) states to np Rydberg states belonging to series converging on the $X^+ \ ^2\Sigma_g^+(v^+=0, N^+=0)$ level of ortho-D₂⁺ and on the $X^+ \ ^2\Sigma_g^+(v^+=0, N^+=1)$ level of para-D₂⁺, respectively. The third column of Table I gives their positions (in cm⁻¹) relative to the 29p2₁ and the 52p1₂ states in the case of ortho- and para-D₂, respectively. These two states are those that were chosen in the measurements using counter-propagating laser beams to determine the ionization energies (see Sec. III B). Adding up the MQDT binding energy and the relative wave number of each Rydberg state measured experimentally yields independent values of the binding energies of the 29p2₁ and the 52p1₂ states, which are listed in the last column of Table I. The uncertainties (one standard deviation) of the binding energies determined in this way are

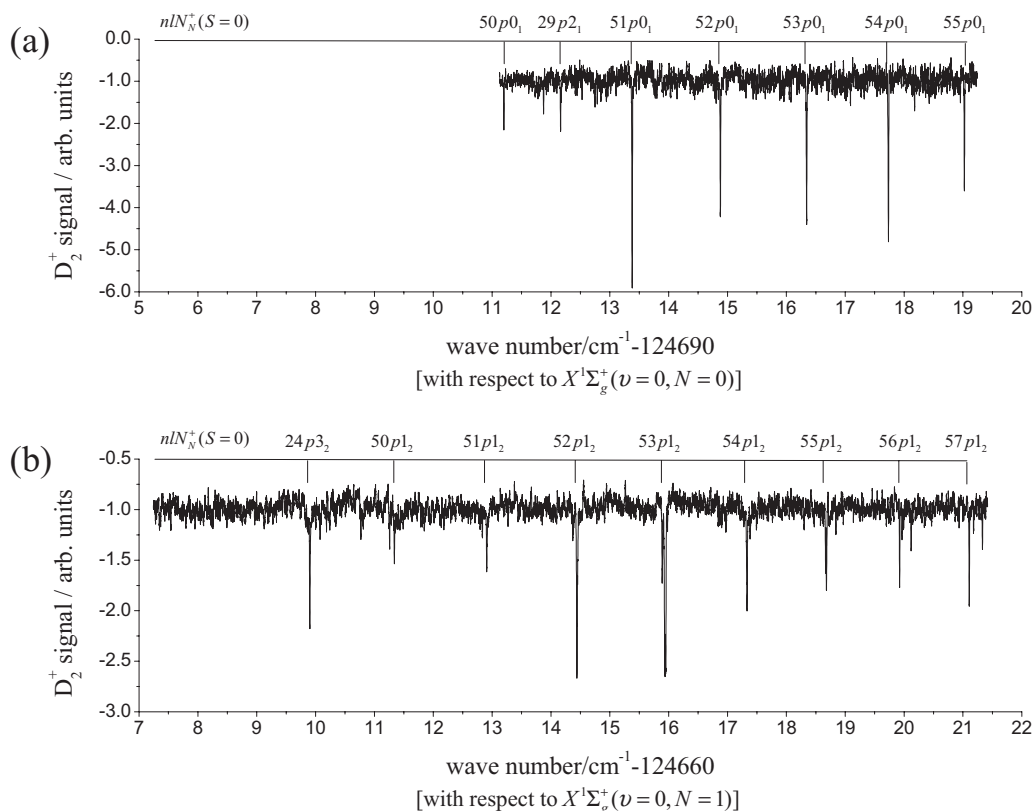


FIG. 2. PFI spectra of Rydberg states of (a) ortho- D_2 and (b) para- D_2 . The relative intensities are very sensitive to experimental conditions and are not reliable.

0.000 58 cm^{-1} and 0.000 74 cm^{-1} for the $29p2_1$ state of ortho- D_2 and the $52p1_2$ state of para- D_2 , respectively, and implicitly include the uncertainties of the MQDT calculation and of the relative frequency calibration of the spectra. The estimated experimental uncertainty is 0.000 80 cm^{-1} , and the standard deviations of the binding energy calculation originates entirely from the experimental uncertainty, which consequently validates the accuracy of the MQDT calculation for the np states: errors in the binding energies calculated by MQDT of the order of 10 MHz would have been detected, and we believe that the MQDT calculations of the np Rydberg states of D_2 are as accurate as those of H_2 , i.e., better than 1 MHz.¹⁴ Note that other weaker transitions were also observed and assigned to transitions to other Rydberg states but were not included into the analysis because of their poor signal-to-noise ratio.

B. Measurements using counterpropagating laser beams

In order to eliminate possible Doppler shifts of the EF Rydberg transition frequencies and determine the ionization energies with better accuracy, the transition wave numbers from the $N=0$ ($N=1$) levels of the $EF\ ^1\Sigma_g^+(v=0)$ state to the $29p2_1(0)$ Rydberg state of ortho- D_2 [$52p1_2(0)$ state of para- D_2] were determined in separate high-precision measurements using counterpropagating laser beams. These two transitions were selected because their fundamental wave numbers are in the vicinity of an I_2 line, the frequency of which had previously been determined to a precision better than 100 kHz using a frequency comb.⁵ An example illus-

trating the calibration of the transition frequency to the $52p1_2(0)$ state of para- D_2 is displayed in Fig. 3.

For each transition, ten measurements were carried out on different days, each measurement consisting of two spectra, one recorded with the 396 nm laser beam propagating parallel, and the other with the 396 nm laser propagating antiparallel to the 201 nm laser beam. The fundamental transition wave numbers determined from these measurements are plotted with their uncertainties in Fig. 4. The center wave

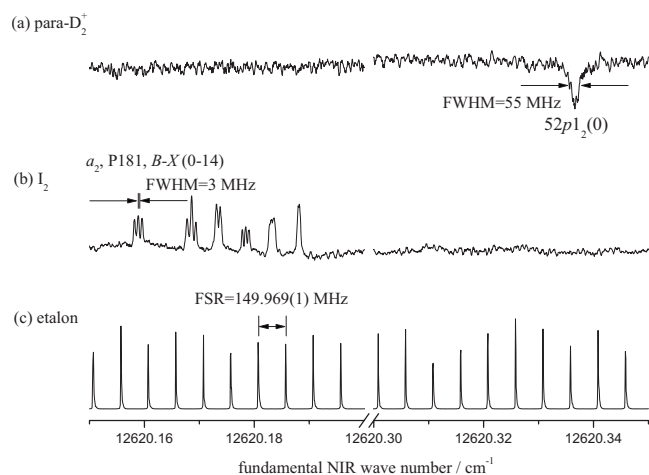


FIG. 3. (a) Spectrum of the transition from the $EF\ ^1\Sigma_g^+(v=0, N=1)$ level to the $52p1_2(S=0)$ level of para- D_2 . [(b) and (c)] I_2 calibration and etalon traces, respectively. The position of the a_2 hyperfine component of the P181, $B-X$ (0-14) rovibronic transition of I_2 was determined to be 378 342 844.89(3) MHz using a frequency comb (Ref. 5) and used for the absolute frequency calibration.

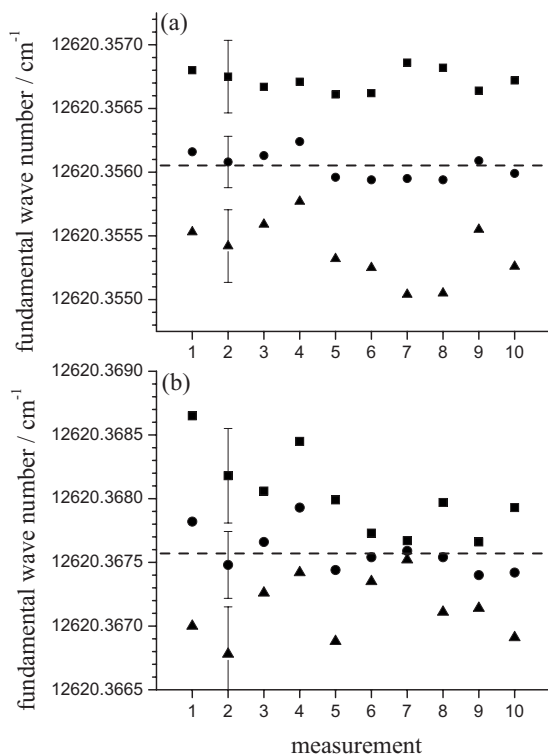


FIG. 4. Distribution of the calibrated fundamental wave numbers of (a) the $29p2_1(0) \leftarrow EF \ 1\Sigma_g^+(v=0, N=0)$ transition of ortho-D₂ and (b) the $52p1_2(0) \leftarrow EF \ 1\Sigma_g^+(v=0, N=1)$ transition of para-D₂. Triangles and squares represent independent measurements with each of the two counter-propagating 396 nm laser beams. Closed circles are the mean values of pairs of measurements. The dashed lines mark the positions of the overall mean values [$12\ 620.356\ 05(11)\ \text{cm}^{-1}$ and $12\ 620.367\ 58(18)\ \text{cm}^{-1}$ for ortho- and para-D₂, respectively.] The size of the experimental uncertainty is indicated by the vertical bars.

numbers of the transitions (full circles) were obtained by taking the average of both measurements. The frequency difference between the two scans of each pair, i.e., twice the Doppler shift, amounted to $\sim 2 \times 50$ MHz, and the mean transition wave numbers are $2 \times 12\ 620.356\ 05(11)\ \text{cm}^{-1}$ and $2 \times 12\ 620.367\ 58(18)\ \text{cm}^{-1}$ for ortho- and para-D₂, respectively, where the numbers in parentheses represent one standard deviation in the unit of the last digit. The frequency shift in the Ti:Sa amplifier has been corrected for in the transition wave numbers listed above. The larger standard deviation of the para-D₂ measurements is attributed to the weaker transition intensities.

C. Error budget for the EF to Rydberg transition wave numbers

The same calibration procedure as used in the previous work on H₂ (Ref. 3) was used for D₂ and its details are not repeated in the body of the article but are presented in Appendix A. Here only the resulting error budget is presented in Table II.

As in our previous investigation of H₂ we evaluated statistical and systematic uncertainties separately. All uncertainties were assumed to be independent of each other and are summarized in Table II. The total statistical and systematic uncertainties were calculated as quadrature summations of all respective contributions. The calibrated EF to Rydberg

transition wave numbers from the measurements displayed in Fig. 4 are given as contributions (2) and (6) in Table III. Their uncertainties are taken as the linear summation of the statistical and systematic uncertainties.

D. Ionization energies, dissociation energy, and the ortho-para separation

Figure 1 illustrates the energy level diagram used in the determination of the ionization energies of ortho- and para-D₂. The numerical values of all relevant energy intervals are listed in Table III and lead to values of the ionization energies of ortho- and para-D₂ of $124\ 745.394\ 07(58)\ \text{cm}^{-1}$ and $124\ 715.003\ 77(75)\ \text{cm}^{-1}$, respectively. These values correspond to the energy separations between the centers of gravity of the hyperfine structure of the $N=0$ (1) level of ortho-D₂ (para-D₂) and the $N^+=0$ (1) level of ortho-D₂⁺ (para-D₂⁺).

Using the ionization energy of D₂ [$E_i(\text{D}_2) \equiv E_i(\text{ortho-D}_2)$] determined in the present work and the previously calculated values of $D_0(\text{D}_2^+)$ [$21\ 711.583\ 34(35)\ \text{cm}^{-1}$, slightly modified from Ref. 8 to take account of higher relativistic and radiative corrections as described in Appendix B] and $E_i(\text{D})$ [$109\ 708.614\ 552\ 99(10)\ \text{cm}^{-1}$, from Ref. 15], the dissociation energy of D₂ is determined from Eq. (1) to be $36\ 748.362\ 86(68)\ \text{cm}^{-1}$ (see Table III). It is important to note that calculations on one-electron systems are much more accurate than on systems with more than one electron. A possible error in the value of $D_0(\text{D}_2^+)$ used here would directly influence the present value of $D_0(\text{D}_2)$.

The ortho-para separation of D₂⁺, i.e., the spacing between the $N^+=0$ and $N^+=1$ levels of the $X^+ \ 2\Sigma_g^+(v^+=0)$ ground state of D₂⁺, was previously determined by *ab initio* calculation to be $29.3910(1)\ \text{cm}^{-1}$.⁸ Combining this result with the ionization energies of ortho- and para-D₂, the ortho-para separation of D₂ can be calculated using Eq. (2) to be $59.781\ 30(95)\ \text{cm}^{-1}$ (see Table III). This value is in excellent agreement with, but more accurate than the value [$59.7805(16)\ \text{cm}^{-1}$] which is calculated using the molecular constants previously derived from an electric quadrupole vibration-rotation spectrum of the fundamental vibrational band of D₂.¹⁶

The overall uncertainties in the ionization energies, the dissociation energy, and the ortho-para separation are determined as quadrature summation of the uncertainties of all energy intervals. The estimated uncertainty of the binding energies of the Rydberg states by MQDT (1 MHz) are based on the previous work on ortho-H₂.¹⁴

IV. DISCUSSION AND CONCLUSIONS

In the present work, the ionization energies of ortho- and para-D₂ have been determined with a precision of 17 and 22 MHz, respectively. These values, derived as combinations of experimentally measured transition frequencies and binding energies of the experimentally accessed Rydberg states calculated based on an MQDT analysis, are confirmed in three different ways:

TABLE II. Error budget in megahertz. In most cases, individual corrections and errors were determined for the frequency of the cw Ti:Sa laser and are then multiplied by 2.

	ortho- D ₂	para- D ₂
rms of 10 measurements using counterpropagating laser beams	$\pm 3.3 \times 2$	$\pm 5.4 \times 2$
Statistical uncertainties		
Uncertainty in the determination of the line centers:		
I ₂ spectra	$\pm 0.35 \times 2$	$\pm 0.37 \times 2$
D ₂ spectra	$\pm 2.8 \times 2$	$\pm 3.5 \times 2$
Nonlinearity of the ring laser scans	$< \pm 1.1 \times 2$	$< \pm 1.1 \times 2$
Residual Doppler shift	$< \pm 0.23$	$< \pm 0.23$
Sum in quadrature (i)	± 6.1	± 7.4
Systematic uncertainties		
Error in linearization resulting from uncertainty of FSR	$\pm 0.043 \times 2$	$\pm 0.046 \times 2$
Uncertainty in the position of the I ₂ reference lines ^a	$< \pm 0.1 \times 2$	$< \pm 0.1 \times 2$
Frequency shift in the Ti:Sa amplifier	$\pm 0.038 \times 2$	$\pm 0.075 \times 2$
Frequency shift in the doubling crystal	$< \pm 0.35$	$< \pm 0.35$
ac Stark shift by the 396 nm laser	$< \pm 1.30 \times 2$	$< \pm 0.51 \times 2$
Frequency shift by the 201 nm laser	$< \pm 1.7 \times 2$	$< \pm 5.4 \times 2$
dc Stark shift by the stray electric fields	$< \pm 5 \times 2$	$< \pm 5 \times 2$
Pressure shift	$< \pm 0.05$	$< \pm 0.05$
Sum in quadrature (ii)	± 10.9	± 14.8
Total uncertainty [(i)+(ii)]	± 17	± 22

^aReference 5.

- (1) Survey spectra of *np* Rydberg states were recorded. The binding energies of selected Rydberg states of ortho-D₂ [$29p2_1(0)$] and para-D₂ [$52p1_2(0)$] were determined as sums of the experimental relative transition wave numbers and the MQDT binding energies corresponding to all Rydberg states observed in the spectra (see Table I). The precision of the calculation (one standard deviation) corresponds to the uncertainty of the frequency calibration, which validates the MQDT calculations (Sec. III A).
- (2) Combining the ionization energies of both ortho- and para-D₂ determined in the present work with previously calculated ortho-para separation of D₂⁺, the ortho-para separation of D₂ was determined and found to be consistent with the previous experimental value of McKellar and Oka.¹⁶
- (3) Control measurements of the transition frequencies from the *EF* state to lower *n* Rydberg states (*n*=39, binding energy ~ 72 cm⁻¹) of both ortho- and para-D₂ were also carried out.¹⁷ At *n*=39 the uncertainties resulting from the stray fields are much reduced, but possible errors in the estimation of the binding energies by MQDT increase. The ionization energies derived as sums of the experimentally measured level energies of the Rydberg states and their binding energies calculated by MQDT agree with those reported in the present paper within the estimated uncertainty. The quantum defects used in the calculations are effective ones, deter-

TABLE III. Energy intervals and determination of the ionization energies, dissociation energy and the ortho-para separation of D₂ in cm⁻¹. The labelling of the energy intervals corresponds to Fig. 1.

	Energy interval	Wave number (cm ⁻¹)	Reference
(1)	$EF \ ^1\Sigma_g^+(v=0, N=0) - X \ ^1\Sigma_g^+(v=0, N=0)$	99 461.449 08(11)	5
(2)	$29p2_1(0) - EF \ ^1\Sigma_g^+(v=0, N=0)$	25 240.712 10(57)	This work
(3)	$X^+ \ ^2\Sigma_g^+(v^+=0, N^+=0) - 29p2_1(0)$ (binding energy)	43.232 89(3)	This work
(4)=(1)+(2)+(3)	$E_i(D_2) \equiv E_i(\text{ortho-D}_2) \equiv [X^+ \ ^2\Sigma_g^+(v^+=0, N^+=0) - X \ ^1\Sigma_g^+(v=0, N=0)]$	124 745.394 07(58)	This work
(5)	$EF \ ^1\Sigma_g^+(v=0, N=1) - X \ ^1\Sigma_g^+(v=0, N=1)$	99 433.716 38(11)	5
(6)	$52p1_2(0) - EF \ ^1\Sigma_g^+(v=0, N=1)$	25 240.735 16(74)	This work
(7)	$X^+ \ ^2\Sigma_g^+(v^+=0, N^+=1) - 52p1_2(0)$ (binding energy)	40.552 23(3)	This work
(8)=(5)+(6)+(7)	$E_i(\text{para-D}_2) \equiv [X^+ \ ^2\Sigma_g^+(v^+=0, N^+=1) - X \ ^1\Sigma_g^+(v=0, N=1)]$	124 715.003 77(75)	This work
	$D_0(D_2^+)$	21 711.583 34(35) ^a	8
	$E_i(D)$	109 708.614 552 99(10)	15
	$D_0(D_2) = E_i(D_2) + D_0(D_2^+) - E_i(D)$	36 748.362 86(68)	This work
(9)	$X^+ \ ^2\Sigma_g^+(v^+=0, N^+=1 - 0)$ (ortho-para separation of D ₂ ⁺)	29.3910(1)	8
(10)=(4)+(9)-(8)	$X \ ^1\Sigma_g^+(v=0, N=1 - 0)$ (ortho-para separation of D ₂)	59.781 30(95)	This work

^aSlightly modified to take account of higher relativistic and radiative corrections (see Appendix B).

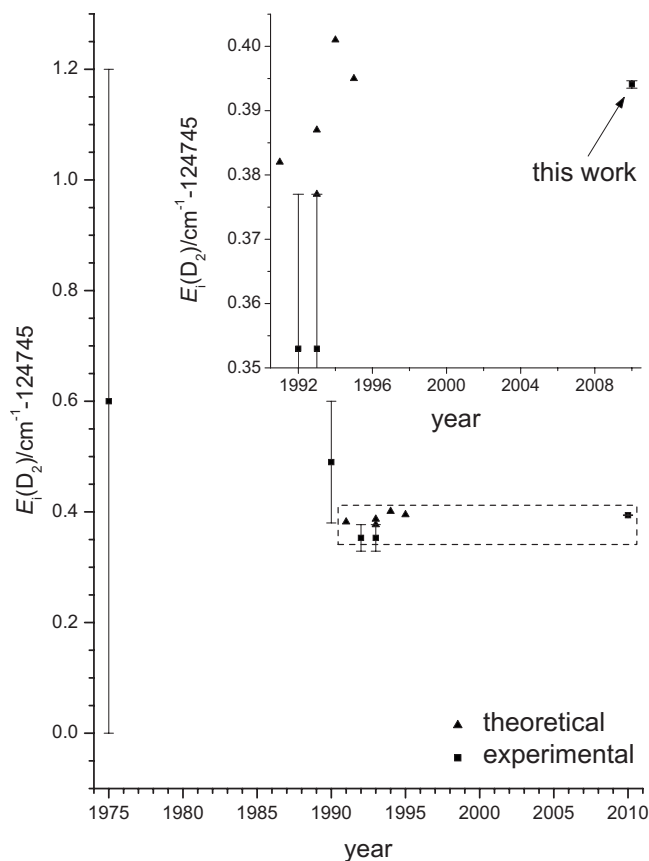


FIG. 5. Values for the ionization energy of D₂ as determined in various studies or combinations thereof. The theoretical values were reported without uncertainties. The inset represents an enlargement of the area surrounded by the dashed line. The numerical values and the references are listed in Table IV.

mined from fits to experimental data using a theoretical model which does not include doubly excited channels and uses a limited number of vibrational channels. That these approximations do not play a significant role in the present determination has been verified to the best of our experimental capabilities (see Refs. 6 and 14 and Table I).

Figure 5 summarizes the results of determinations, by various methods, of the ionization energy of D₂ over the past 35 years. The numerical values are also listed in Table IV. Because of the relationship between the dissociation and ionization energies of D₂ [Eq. (1)], the recommended value of the dissociation energy evolved in a very similar manner. The dissociation energy of D₂ was determined in the present work as a hybrid experimental-theoretical value. Comparing with the most recent experimental result [36 748.343(10) cm⁻¹, Ref. 4], the present value for the dissociation energy of D₂ [36 748.362 86(68) cm⁻¹] is more precise by more than one order of magnitude but differs by two standard deviations of the previous measurement. Our new value is in remarkable agreement with the most recent theoretical value [36 748.3633(9) cm⁻¹, Ref. 2]. The same excellent agreement was found between our value of the dissociation energy of H₂ [36 118.069 62(37) cm⁻¹, Ref. 3] and the value derived *ab initio* [36 118.0695(10) cm⁻¹, Ref. 2].

TABLE IV. $E_i(D_2)$ as determined in various experimental and theoretical studies or combinations thereof, in cm⁻¹.

Year	Expt.	Theor.	Reference
1975	124 745.6(6) ^a		28
1990	124 745.49(11)		29
1991		124 745.382	30,31
1992	124 745.353(24)		32,33
1993	124 745.353(24)		34
1993		124 745.377	35
1993		124 745.387	36
1994		124 745.401	37
1995		124 745.395	38
2010	124 745.394 07(58)		This work

^aA correction of -1.0 cm⁻¹ was included to account for the pressure shift (see Ref. 33).

Our present work on D₂ hence serves as an independent verification of the theoretical calculations in Ref. 2. Because the experimental uncertainties in the values of the dissociation energies of H₂ and D₂ are smaller than those of the best *ab initio* calculations, they represent a benchmark for future calculations.

ACKNOWLEDGMENTS

This work was financially supported by the European Research Council (ERC Grant No. 228286) and the Swiss National Science Foundation under project No. 200020-116245. Additional support from the Swiss Academy of Technical Sciences, Program PHC Germaine de Staël Nr. 2008-35 is also acknowledged.

APPENDIX A: EXPERIMENTAL ERRORS AND UNCERTAINTIES

This appendix provides the information on the different contributions to the uncertainties in the determination of the frequencies of the transitions from the $EF\ ^1\Sigma_g^+(v=0, N=0,1)$ states to the np Rydberg states of ortho- and para-D₂ located below the $X^+ \ ^2\Sigma_g^+(v^+=0, N^+=0,1)$ ionization thresholds.

1. Statistical uncertainties

Determination of the line centers. The central wave numbers of the I₂ calibration lines were determined by fitting Lorentzian line shapes to the recorded line profiles. The central wave numbers of the EF to Rydberg transitions of D₂ were obtained by fitting Gaussian line shapes. The averaged uncertainties (one standard deviation) in determining the center frequencies are 2×0.35 MHz (2×0.37 MHz) and 2×2.8 MHz (2×3.5 MHz) for I₂ and D₂ transitions in the case of ortho-D₂ (para-D₂), respectively. The larger uncertainty in the case of para-D₂ results from the weaker nature of the transitions as discussed in Sec. III B.

Nonlinearity of the ring laser. The maximum deviation of the NIR readout frequency of the Ti:Sa ring laser from the actual frequency resulting from the nonlinearity of the scans occurs at the midpoint between two neighboring monitor etalon fringes. From the maximal relative error of $\sim 1.5\%$ over

one free spectral range (FSR) of the monitor etalon, we conclude that the frequency uncertainty resulting from the non-linearity is always smaller than $(1/2)\text{FSR} \times 1.5\% = 1.1$ MHz in the NIR and smaller than 2.2 MHz in the UV.

Doppler shift. Although the method of counterpropagating laser beams was employed (see Sec. III B), there still could be a small residual Doppler shift caused by an imperfect alignment of the two 396 nm laser beams. The common beam path of the two beams is $L \sim 3.5$ m. If two beams deviate by $\delta = 0.5$ mm (which is still easily resolvable by eye) at the extremity of the common path, the Doppler shift $\Delta\nu_{\text{Doppler}}$ is

$$\Delta\nu_{\text{Doppler}} = \frac{1}{2} \cdot \frac{v_{D_2}}{c} \cdot \frac{\delta}{L} \cdot \nu_0 = 0.23 \text{ MHz}, \quad (\text{A1})$$

where $v_{D_2} = 1260$ m/s is the speed of D_2 in the jet expansion and ν_0 is the transition frequency. The Doppler shift is therefore smaller than 0.23 MHz.

2. Systematic errors and uncertainties

Uncertainty of the FSR. The FSR of the etalon was determined to be 149.9691(13) MHz in nine measurements carried out on nine days. Multiplying the uncertainty of the FSR by the number of FSRs separating the I_2 line that was used for calibration [the a_2 hyperfine component of the P181, $B-X$ (0-14) rovibronic transition at 12 620.158 873(1) cm^{-1}] from the position of the Rydberg transitions gives uncertainties of 2×0.043 and 2×0.046 MHz in the transition frequencies of ortho- and para- D_2 , respectively.

I_2 calibration by frequency comb. This uncertainty is less than 0.1 MHz in the NIR as explained in Ref. 5.

Frequency shifts occurring in the Ti:Sa amplifier. The frequency shifts occurring in the Ti:Sa amplifier, $-4.736(38)$ MHz for ortho- D_2 measurements and $-6.901(75)$ MHz for para- D_2 measurements, were determined simultaneously with the measurements described in Sec. III B and have already been corrected for in the transition wave numbers presented in Fig. 4. The larger frequency shift for the para- D_2 measurements and its larger uncertainty result from the fact that a higher 396 nm laser power had to be used to compensate for the weaker signal, which could only be achieved by pumping the Ti:Sa crystals with higher Nd:YAG laser intensities.

Frequency shifts in the doubling crystal. The frequency shifts arising in frequency doubling have been estimated to be less than 0.35 MHz in our previous study.³

ac Stark shifts caused by the 396 nm laser power. To estimate the ac Stark shift, the D_2 spectra were recorded at different laser powers and hence different intensities of the 396 nm laser and zero-intensity positions were estimated in a linear extrapolation. The uncertainties associated with the extrapolations are estimated as the product of the slope and the laser powers used in the measurements.

Frequency shifts caused by the 201 nm laser power. The transition frequencies were found to be dependent on the 201 nm laser power. When the average laser power is low (< 4.5 mW, corresponding to average pulse energies of 180 μJ); the estimated beam waist in the interaction region is

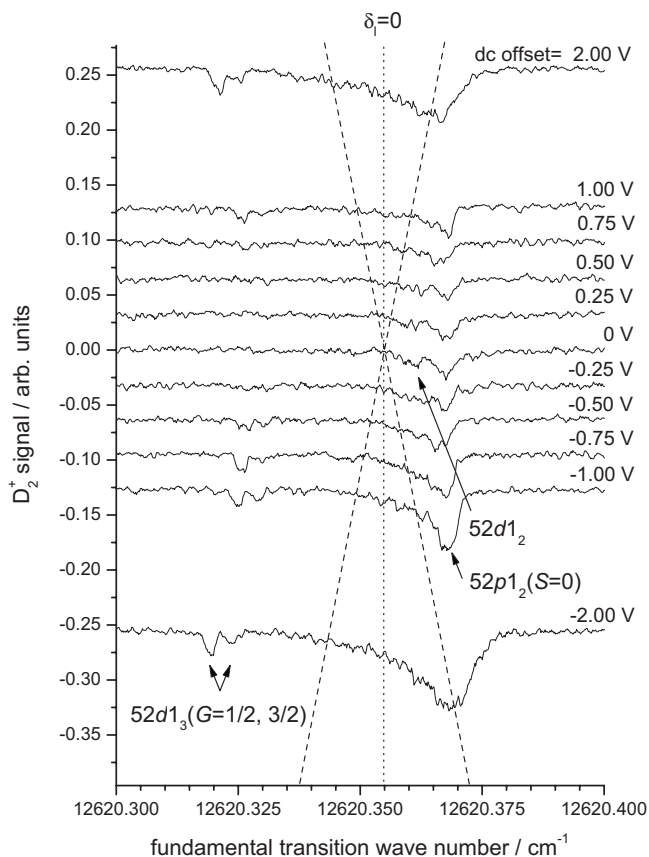


FIG. 6. Spectra of para- D_2 recorded in the vicinity of the $52p_{12}(0) \leftarrow EF \ ^1\Sigma_g^+(v=0, N=1)$ transition with different dc voltage offsets applied across the 7.8-cm-long extraction region. The dotted line indicates the zero-field position of high- ℓ Rydberg states with $\delta_\ell=0$. The dashed lines indicate the positions of the extreme red- and blueshifted Stark levels (see text). The spectra have been shifted along the vertical axis so that the origin of their intensity scale corresponds to the value of the applied dc electric field in V/cm.

~ 1 mm²), the transition frequencies remain constant, but they start increasing at laser powers beyond 4.5 mW. Because we also observed these frequency shifts in experiments in which the 396 nm laser was delayed with respect to the 201 nm laser, they cannot arise from an ac Stark shift induced by the 201 nm laser. Instead, we attribute them to the stray electric fields caused by the ions generated by the 201 nm laser in a (2+1) resonance-enhanced multiphoton ionization process. The measurements using counterpropagating laser beams presented in Fig. 4 were carried out at low 201 nm laser power (~ 1.5 mW for ortho- D_2 and ~ 2.0 mW for para- D_2) so that no frequency corrections needed to be made. Nevertheless, it was necessary to include additional uncertainties of 3.5 MHz for ortho- D_2 and 10.8 MHz for para- D_2 , determined in the same way as for the ac Stark shift caused by the 396 nm laser power.

dc Stark shifts caused by stray electric fields. The effects of dc electric fields of different magnitudes and polarities were investigated by applying dc voltages across the 7.8-cm-long stack of cylindrical plates surrounding the ionization region. Figure 6 shows the effect of these dc voltages on the spectrum of para- D_2 . The transition to the $52d_{12}$ state is always observable and its intensity increases with increasing electric field. The linewidth increases as well, presumably

TABLE V. Re-evaluation of the dissociation energy of D_2^+ including all relativistic and radiative corrections up to order $R_\infty\alpha^4$ and the leading two terms of order $R_\infty\alpha^5$. In this treatment one assumes that the perturbation series is convergent. The estimation is based on calculations of Moss (Refs. 8, 24, 25, and 39) on H_2^+ , HD^+ , and D_2^+ , of Korobov (Refs. 26 and 27) on H_2^+ and HD^+ , and of CODATA (Ref. 7) on H and D. The upper part of the table gives the ground state energy of the respective species and their corrections. All values are in units of cm^{-1} . The correction terms are listed in Refs. 26 and 27. The corrections are: RR=relativistic and recoil, NS=nuclear size, SAV=self-energy, anomalous magnetic moment, and vacuum polarization, and TP=transverse photon exchange.

	Reference	Nonrel. energy	$R_\infty\alpha^2$		$R_\infty\alpha^3$		$R_\infty\alpha^4$	$R_\infty\alpha^5$	total correction
			RR	NS	SAV	TP			
$E(H)$	7	-109 677.583 41	-1.460 95	0.000 04	0.270 68	0.000 08	0.001 94	-0.000 12	-1.188 33
	24		-1.460 92		0.270 66				-1.190 26
$E(D)$	7	-109 707.426 59	-1.460 95	0.000 24	0.270 89	0.000 04	0.001 94	-0.000 11	-1.187 96
	25		-1.460 92		0.270 88				-1.190 04
$E_0(H_2^+)$	26, 27	-131 056.875 75	-1.599 55	0.000 05	0.350 83	0.000 10	0.002 49	-0.000 15	-1.246 23
	24		-1.598 82		0.350 76				-1.248 07
Deviations			-0.000 73		0.000 07				
$E(HD^+)$	26, 27	-131 223.436 26	-1.602 10	0.000 18	0.351 60	0.000 07	0.002 50	-0.000 15	-1.247 89
	25		-1.601 52		0.351 58				-1.249 99
Deviations			-0.000 58		0.000 02				
$E(D_2^+)$	39	-131 418.947 71							
	8		-1.604 82		0.352 48				-1.252 32
Estimated deviations			-0.000 58(30) ^a		0.000 02(10) ^a				
Estimated corrections			-1.605 40(32) ^b	0.000 31(5) ^c	0.352 50(14) ^b	0.000 05(3) ^c	0.002 50(3) ^c	-0.000 15(3) ^c	-1.250 19(35)
$D_0(H_2^+)$	24	21 379.292 28	0.1379		-0.0801				0.057 82
$=E(H)-E(H_2^+)$	7, 26, 27	21 379.292 34	0.138 60	-0.000 01	-0.080 15	-0.000 02	-0.000 56	0.000 04	0.057 90
$D_0(HD^+)$	25	21 516.0096	0.1406		-0.0807				0.0600
$=E(D)-E(HD^+)$	7, 26, 27	21 516.009 67	0.141 14	0.000 06	-0.080 71	-0.000 03	-0.000 56	0.000 04	0.059 93
$D_0(D_2^+)$	8	21 711.521 05	0.1439		-0.0816				0.062 25
Estimated $D_0(D_2^+)$		21 711.521 12 ^d	0.144 45(32)	-0.000 07(5)	-0.081 61(14)	-0.000 01(3)	-0.000 57(3)	0.000 04(3)	0.062 22(35)

^aTaken to be the same as for HD^+ but including an uncertainty larger than the difference between the H_2^+ and HD^+ values.

^bSum of the value from Ref. 8 and the estimated deviation.

^cExtrapolated linearly from the values of H_2^+ and HD^+ .

^dDetermined using the value of $E(D_2^+)$ from Ref. 39 and the most recent value of $E(D)$ (Ref. 7).

because of Stark splittings and mixing with Stark manifolds of high- ℓ states. Because of the $\Delta\ell = \pm 1$ selection rule of ℓ -mixing by electric fields, the $52p$ state mixes first with the $52d$ state, and then with high- ℓ states via the $52d$ state. The zero-field positions of high- ℓ states (with quantum defect $\delta_\ell = 0$) and the extreme red- and blueshifted Stark levels are indicated by the dotted and dashed lines in Fig. 6. The Stark shifts of these levels are calculated using the formula $\Delta E_n = \pm (3/2)Fn^2$ (in atomic units), where F is the electric field. At a dc voltage of 2 V, the $52p$ and $52d$ levels are completely immersed in the high- ℓ manifold of Stark states and the Stark spectra are dominated by a broad asymmetric line. Two new peaks appear at dc offsets beyond 0.25 V and can be assigned to the transitions from the EF state to the $52d1_3(G=1/2)$ and $52d1_3(G=3/2)$ Rydberg states based on the results of a previous laser experiment.¹⁸ For transitions to np levels of both ortho- and para- D_2 , no dependence of the transition frequencies on the electric field was observable at low electric fields. [A quadratic frequency shift with respect to the offset voltage^{19,20} was observed for the transitions to the $52d1_3(G=1/2, 3/2)$ states.] Consequently, no correction was needed for the dc Stark shift, but an uncertainty of 2×5 MHz = 10 MHz was included to account for the shift at a field of ± 250 mV/7.8 cm. It is, however, certain that the stray electric field present during the measurements using counterpropagating laser beams summarized in Fig. 4 was smaller.

Pressure shift. Herzberg and Jungen²¹ determined the magnitude of the pressure shift for high- n Rydberg states of H_2 to be 5.7 ± 0.5 cm⁻¹/amagat, which is expected to be the same for D_2 . From the estimate of $\sim 10^{13}$ cm⁻³ for the D_2 number density, we determine the pressure shift to be less than +0.1 MHz with an uncertainty of ± 0.05 MHz. This pressure shift thus makes a close to negligible contribution to the error budget.

APPENDIX B: RE-EVALUATION OF THE DISSOCIATION ENERGY OF D_2^+

In our derivation of the dissociation energy of D_2 we rely on the dissociation energy of D_2^+ [see Eq. (1)]. This quantity has been calculated in 1993 by Moss to be 21 711.5833 cm⁻¹.⁸ In his calculations, Moss included relativistic corrections of order $R_\infty\alpha^2$ (taken from Ref. 22) and radiative corrections of order $R_\infty\alpha^3$ (using the Bethe logarithm evaluated in Ref. 23). In similar calculations he also determined the dissociation energies of other rovibronic states of H_2^+ , HD^+ , and D_2^+ , derived transition frequencies and compared his results with available experimental data.^{8,24,25} The agreement was in most cases better than the estimated experimental uncertainty of 0.001 cm⁻¹.

A re-evaluation of the dissociation energy of D_2^+ was carried out based on the recent work of Korobov on H_2^+ and HD^+ , in which relativistic and radiative corrections of order up to $R_\infty\alpha^4$ (including also the leading $R_\infty\alpha^5$ terms) were calculated.^{26,27} The results of this reevaluation are summarized in Table V, where relativistic and radiative corrections to the energies of H, D, H_2^+ , HD^+ , and D_2^+ , and the dissociation energies of H_2^+ , HD^+ , and D_2^+ are given. While the radia-

tive corrections of order $R_\infty\alpha^3$ are in good agreement with those used by Moss,^{24,25} there is a discrepancy of -0.0007 cm⁻¹ and -0.0005 cm⁻¹ in the sum of the relativistic and the recoil corrections of order $R_\infty\alpha^2$ in the dissociation energies of H_2^+ and HD^+ , respectively. This discrepancy is almost fully compensated by the radiative corrections of order $R_\infty\alpha^4$,^{26,27} leading to an excellent but coincidental agreement in the value of the overall correction. Based on the corrections needed for H_2^+ and HD^+ , we estimated the corrections for the dissociation energy of D_2^+ as detailed in Table V. The resulting dissociation energy for D_2^+ is 21 711.583 34(35) cm⁻¹, which is almost identical to the value reported by Moss.⁸ As for H_2^+ and HD^+ the agreement results from an almost exact but coincidental compensation.

The rotational energy level structure of the vibronic ground state of D_2^+ was also taken from Ref. 8 and used in the MQDT calculations (see Sec. III A) and in the determination of the ortho-para separation of D_2 [see Eq. (2)]. Relativistic and radiative corrections are almost an order of magnitude smaller for the rotational energies than they are for the dissociation energy so that the values of Moss^{24,25} and Korobov^{26,27} for H_2^+ and HD^+ are in perfect agreement. The positions of the rotational energy levels of D_2^+ were therefore taken without change from Ref. 8.

- ¹H. Primas and U. Müller-Herold, *Elementare Quantenchemie* (Teubner Studienbücher, Stuttgart, 1984). Section 5.3 (“Fakten und Zahlen: Die Geschichte des Wasserstoff-Moleküls”) gives a complete account of the early efforts invested in the quantitative comparison of experimental and theoretical values of the dissociation energy of H_2 and explains in detail how studies of molecular hydrogen contributed to establish the validity of molecular quantum mechanics and to understand chemical bonds physically.
- ²K. Piszczatowski, G. Łach, M. Przybytek, J. Komasa, K. Pachucki, and B. Jeziorski, *J. Chem. Theory Comput.* **5**, 3039 (2009).
- ³J. Liu, E. J. Salumbides, U. Hollenstein, J. C. J. Koelemeij, K. S. E. Eikema, W. Ubachs, and F. Merkt, *J. Chem. Phys.* **130**, 174306 (2009).
- ⁴Y. P. Zhang, C. H. Cheng, J. T. Kim, J. Stanojevic, and E. E. Eyler, *Phys. Rev. Lett.* **92**, 203003 (2004).
- ⁵S. Hannemann, E. J. Salumbides, S. Witte, R. T. Zinkstok, E.-J. van Duijn, K. S. E. Eikema, and W. Ubachs, *Phys. Rev. A* **74**, 062514 (2006).
- ⁶H. A. Cruse, Ch. Jungen, and F. Merkt, *Phys. Rev. A* **77**, 042502 (2008).
- ⁷P. J. Mohr, B. N. Taylor, and D. B. Newell, *Rev. Mod. Phys.* **80**, 633 (2008).
- ⁸R. E. Moss, *J. Chem. Soc., Faraday Trans.* **89**, 3851 (1993).
- ⁹R. Seiler, Th. Paul, M. Andrist, and F. Merkt, *Rev. Sci. Instrum.* **76**, 103103 (2005).
- ¹⁰Th. A. Paul and F. Merkt, *J. Phys. B* **38**, 4145 (2005).
- ¹¹H. Knöckel, B. Bodermann, and E. Tiemann, *Eur. Phys. J. D* **28**, 199 (2004).
- ¹²Th. A. Paul, J. Liu, and F. Merkt, *Phys. Rev. A* **79**, 022505 (2009).
- ¹³I. Reinhard, M. Gabrysch, B. F. von Weikersthal, K. Jungmann, and G. zu Putlitz, *Appl. Phys. B: Lasers Opt.* **63**, 467 (1996).
- ¹⁴A. Osterwalder, A. Wüest, F. Merkt, and Ch. Jungen, *J. Chem. Phys.* **121**, 11810 (2004).
- ¹⁵See: <http://physics.nist.gov/hdel> (The energy levels of hydrogen and deuterium given in this database include all corrections detailed in Ref. 7. The fundamental constants used in the calculations are taken from CODATA 2002).
- ¹⁶A. R. W. McKellar and T. Oka, *Can. J. Phys.* **56**, 1315 (1978).
- ¹⁷D. Sprecher, J. Liu, and F. Merkt (unpublished).
- ¹⁸Th. A. Paul, H. A. Cruse, H. J. Wörner, and F. Merkt, *Mol. Phys.* **105**, 871 (2007).
- ¹⁹M. Schäfer and F. Merkt, *Phys. Rev. A* **74**, 062506 (2006).
- ²⁰A. Osterwalder and F. Merkt, *Phys. Rev. Lett.* **82**, 1831 (1999).
- ²¹G. Herzberg and Ch. Jungen, *J. Mol. Spectrosc.* **41**, 425 (1972).
- ²²M. H. Howells and R. A. Kennedy, *J. Chem. Soc., Faraday Trans.* **86**, 3495 (1990).

- ²³R. Bukowski, B. Jeziorski, R. Moszyński, and W. Kołos, *Int. J. Quantum Chem.* **42**, 287 (1992).
- ²⁴R. E. Moss, *Mol. Phys.* **80**, 1541 (1993).
- ²⁵R. E. Moss, *Mol. Phys.* **78**, 371 (1993).
- ²⁶V. I. Korobov, *Phys. Rev. A* **74**, 052506 (2006).
- ²⁷V. I. Korobov, *Phys. Rev. A* **77**, 022509 (2008).
- ²⁸S. Takezawa and Y. Tanaka, *J. Mol. Spectrosc.* **54**, 379 (1975).
- ²⁹Ch. Jungen, I. Dabrowski, G. Herzberg, and M. Vervloet, *J. Chem. Phys.* **93**, 2289 (1990).
- ³⁰W. Kołos, K. Szalewicz, and H. J. Monkhorst, *J. Chem. Phys.* **84**, 3278 (1986).
- ³¹L. Wolniewicz and T. Orlikowski, *Mol. Phys.* **74**, 103 (1991).
- ³²J. M. Gilligan and E. E. Eyler, *Phys. Rev. A* **46**, 3676 (1992).
- ³³Ch. Jungen, I. Dabrowski, G. Herzberg, and M. Vervloet, *J. Mol. Spectrosc.* **153**, 11 (1992).
- ³⁴D. Shiner, J. M. Gilligan, B. M. Cook, and W. Lichten, *Phys. Rev. A* **47**, 4042 (1993).
- ³⁵W. Kołos and J. Rychlewski, *J. Chem. Phys.* **98**, 3960 (1993).
- ³⁶L. Wolniewicz, *J. Chem. Phys.* **99**, 1851 (1993).
- ³⁷W. Kołos, *J. Chem. Phys.* **101**, 1330 (1994).
- ³⁸L. Wolniewicz, *J. Chem. Phys.* **103**, 1792 (1995).
- ³⁹R. E. Moss, *J. Phys. B* **32**, L89 (1999).